A role for myosin VI in postsynaptic structure and glutamate receptor endocytosis

Emily Osterweil,[1] David G. Wells,[1] and Mark S. Mooseker[1,2,3]

[1]Department of Molecular, Cellular and Developmental Biology, [2]Department of Cell Biology, and [3]Department of Pathology, Yale University, New Haven, CT 06511

Myosin VI (Myo6) is an actin-based motor protein implicated in clathrin-mediated endocytosis in nonneuronal cells, though little is known about its function in the nervous system. Here, we find that Myo6 is highly expressed throughout the brain, localized to synapses, and enriched at the postsynaptic density. Myo6-deficient (*Snell's waltzer*; *sv/sv*) hippocampus exhibits a decrease in synapse number, abnormally short dendritic spines, and profound astrogliosis. Similarly, cultured *sv/sv* hippocampal neurons display decreased numbers of synapses and dendritic spines, and dominant-negative disruption of Myo6 in wild-type hippocampal neurons induces synapse loss. Importantly, we find that *sv/sv* hippocampal neurons display a significant deficit in the stimulation-induced internalization of α-amino-3-hydroxy-5-methyl-4-isoxazole propionic acid–type glutamate receptors (AMPARs), and that Myo6 exists in a complex with the AMPAR, AP-2, and SAP97 in brain. These results suggest that Myo6 plays a role in the clathrin-mediated endocytosis of AMPARs, and that its loss leads to alterations in synaptic structure and astrogliosis.

Introduction

In the mature brain, excitatory transmission occurs with the presynaptic release of glutamate, which binds and activates receptors clustered at the postsynaptic density (PSD). In the majority of neurons, these excitatory synapses are made at dendritic spines, or small protrusions of dendrite. It is thought that the modulation of glutamate receptor expression at the PSD results in long-lasting changes in synaptic strength, though the mechanisms behind this are poorly understood (Malinow and Malenka, 2002). Recently, it has been suggested that F-actin, the major cytoskeletal component of the postsynaptic terminal, is essential for this process. Indeed, depolymerization of F-actin has been shown to disrupt signaling through both the α-amino-3-hydroxy-5-methyl-4-isoxazole propionic acid (AMPA)–type glutamate receptor (AMPAR) and the *N*-methyl-D-aspartate–type glutamate receptor (NMDAR), which are the two ionotropic receptors responsible for the majority of fast glutamatergic transmission (Rosenmund and Westbrook, 1993; Kim and Lisman, 1999). However, the link between glutamate receptor activity and F-actin has yet to be explored in depth.

Correspondence to Emily Osterweil: emily.osterweil@yale.edu

Abbreviations used in this paper: AMPA, α-amino-3-hydroxy-5-methyl-4-isoxazole propionic acid; AMPAR, AMPA-type glutamate receptor; dnM6, dominant-negative Myo6; DOC, deoxycholate; GaR, goat anti–rabbit; GFAP, glial fibrillary acidic protein; IP, immunoprecipitation; LTD, long-term depression; Myo6, myosin VI; Myo7a, myosin VIIa; NMDAR, *N*-methyl-D-aspartate–type glutamate receptor; PSD, postsynaptic density; Tf, transferrin; TTX, tetrodotoxin; TX, Triton X-100.

Myosins are motor proteins that move on F-actin, using the hydrolysis of ATP, transporting vesicles, organelles, protein complexes, and mRNA, to various sites in the cell (Mermall et al., 1998). In humans, there are nearly 40 myosin genes grouped into 12 distinct classes; together, they are essential for a multitude of cellular processes, including endocytosis, exocytosis, and cell motility (Mermall et al., 1998; Berg et al., 2001). Underscoring their importance, mutations in myosin genes have been linked to a variety of diseases in humans, including deafness, blindness, and cardiac myopathy (Redowicz, 2002; Mohiddin et al., 2004). Although multiple myosins have been found in neurons (Bridgman, 2004), their functions there are largely unknown. One such myosin is myosin VI (Myo6). In nonneuronal cells, Myo6 has been implicated in clathrin-mediated endocytosis and vesicle trafficking (Buss et al., 2001; Hasson, 2003). Myo6 is considered unique, as it moves toward the slow-growing (minus) ends of actin filaments (Wells et al., 1999), which tend to be oriented toward the cell center. In contrast, all other native myosins studied have been shown to move toward the fast-growing (plus) ends of F-actin. It has been suggested that its directionality allows for Myo6 at the plasma membrane to pull endocytic vesicles inward using force generated by its movement on F-actin (Hasson, 2003).

Consistent with this suggestion, Myo6 has been localized to sites of endocytosis in kidney-proximal tubule cells (Biemesderfer et al., 2002), intestinal enterocytes (Heintzelman et al., 1994), and inner ear hair cells (Hasson et al., 1997). In

The Journal of Cell Biology, Vol. 168, No. 2, January 17, 2005 329–338
http://www.jcb.org/cgi/doi/10.1083/jcb.200410091

addition, Myo6 interacts with the clathrin adaptor protein AP-2 via the linker protein Dab2, and experiments using a dominant-negative Myo6 (dnM6) show that Myo6 is essential for clathrin- and AP-2–mediated endocytosis, as well as for the trafficking of uncoated endocytic vesicles (Buss et al., 2001; Morris et al., 2002; Aschenbrenner et al., 2003). However, evidence of an endocytic disruption in Myo6-deficient (*Snell's waltzer*; *sv/sv*) cells is less direct. The inner ear hair cells of the *sv/sv* mouse exhibit fused stereocilia, and this fusion may be the result of inefficient endocytosis at their base (Self et al., 1999). In addition, recent experiments show that fibroblasts cultured from *sv/sv* mice display abnormal vesicular trafficking at the Golgi apparatus (Warner et al., 2003).

In the present study, we find that Myo6 is expressed throughout the brain, present at synapses, and biochemically enriched with the PSD. Myo6 association with the PSD is not dependent on F-actin interaction. Examination of *sv/sv* brain reveals decreases in synapse number and dendritic spine length in the hippocampus, as well as widespread astrogliosis. In addition, cultured *sv/sv* hippocampal neurons display decreases in both synapses and numbers of dendritic spines, and wild-type neurons expressing dnM6 similarly display synapse loss. Interestingly, we find that both AMPA- and insulin-induced AMPAR internalization are disrupted in hippocampal neurons cultured from *sv/sv* mice. In control neurons, inhibition of clathrin-mediated endocytosis disrupts AMPAR internalization to the same extent. Supporting this, Myo6 exists in a complex with the AMPAR and SAP97, a putative AMPAR trafficking protein, in rat brain (Wu et al., 2002), and we find that this complex also contains AP-2. This interaction is not seen with the NMDAR, which suggests that Myo6 specifically interacts with endocytic AMPARs. Consistent with this, no deficit is seen in constitutive transferrin (Tf) receptor internalization in *sv/sv* neurons. To our knowledge, these results constitute the first time a deficit in clathrin-mediated endocytosis has been seen in *sv/sv* cells.

Results

Myo6 is expressed throughout the brain

Immunostaining of adult mouse brain shows that Myo6 is enriched in multiple layers of the cortex, hippocampus, and cerebellum (Fig. 1 A). Hippocampal expression is the same throughout areas CA1, CA2, and CA3, and the dentate gyrus, whereas cerebellar expression is highest in the molecular layer (Fig. 1, B and C). Myo6 is expressed at a high level in the neuropil, in contrast to myelinated fiber tracts, where expression is low. In addition to its distribution, we examined the expression of Myo6 during brain development. Western blotting of whole brain homogenates reveals that there is no significant change in total brain Myo6 expression from postnatal day 1 to adulthood (Fig. 1 D).

Myo6 is present at synapses and enriched at the PSD

To explore its subcellular distribution, we immunostained mature rat hippocampal neurons for Myo6. Myo6 is seen throughout the cell, and is highly expressed at the perinuclear region and in dendrites, where it is concentrated in discrete puncta. These puncta partially colocalize with the synaptic marker PSD-95, indicating that Myo6 is present at synapses (Fig. 2 A). This partial, rather than complete, colocalization pattern is not surprising, as myosins are dynamic and are often found in many different subcellular regions. To examine the enrichment of Myo6 at synapses, we performed a biochemical fractionation protocol designed to isolate the PSD component from brain. This procedure yields a synaptosome fraction, consisting of resealed pre- and postsynaptic terminals, and a purified PSD fraction (Dosemeci and Reese, 1993). Western blot analyses (loaded equal protein) show that Myo6 is enriched in the PSD fraction, though it is also present in both the homogenate and synaptosome fractions (Fig. 2 B). To determine whether this enrichment exists in specific brain regions, we isolated PSD fractions from the cortex, hippocampus, and cerebellum. These experiments show that Myo6 is enriched with the PSD in all three regions, with the greatest enrichment seen in the cortex (Fig. 2 B). The low expression of the NMDAR in the cerebellum is consistent with previous studies (Yamada et al., 2001).

The enrichment of Myo6 at the PSD could be mediated by its affinity for F-actin, alone. Conversely, Myo6 could interact with other PSD constituents in addition to F-actin. To explore this possibility, we performed ATP extraction experiments on isolated PSD fractions. For many myosins, including Myo6, affinity for actin is decreased in the presence of ATP (Hasson and Mooseker, 1994). PSD fractions were extracted with buffer in the absence or presence of ATP, and the resultant supernatant and pellet fractions were examined. ATP treatment of isolated PSD fractions failed to solubilize the majority of Myo6 (Fig. 2 C). This indicates that Myo6 interacts with other proteins at the PSD, in addition to F-actin. In contrast, ATP treatment of Triton X-100 (TX)–permeabilized synaptosomes resulted in the release of the majority of Myo6 from the pellet

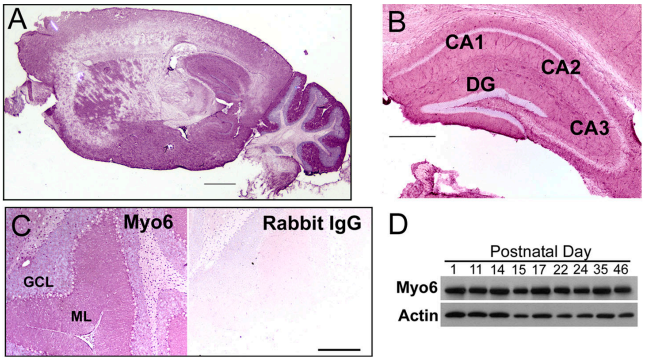

Figure 1. **Myo6 expression in brain.** (A–C) Adult mouse brain sections were stained for Myo6. (A) Sagittal section shows Myo6 is expressed throughout the brain. Higher magnification images of individual brain regions show that Myo6 is highly expressed in (C) the cerebellar molecular (ML) and granule cell (GCL) layers (control nonimmune IgG also shown), and (B) hippocampal areas CA1, CA2, and CA3, and the dentate gyrus (DG). Minimal contrast/brightness adjustment was performed. (D) Western blotting of brain homogenates from mice ages postnatal day 1 to 46 (loaded equal protein) reveals that the expression of Myo6 in whole brain does not change from birth to adulthood. Bars: (A) 1 mm; (B) 0.5 mm; (C) 0.25 mm.

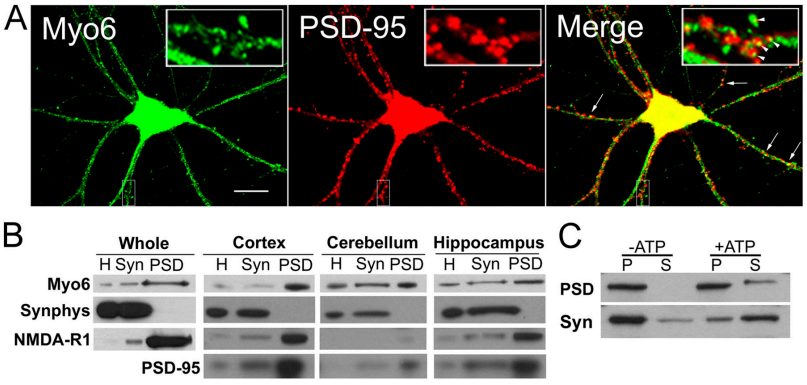

Figure 2. **Myo6 is partially localized to synapses and associated with the PSD in an actin-independent manner.** (A) Hippocampal neurons (at 20 d) were costained for Myo6 and the synapse marker PSD-95, revealing Myo6 localization throughout the cell body and dendrite shaft and in clusters that partially overlap with PSD-95 puncta (arrows). Insets show enlarged regions of dendrite. Arrowheads indicate areas of colocalization. Bar, 10 μm. (B) Western blots of homogenate (H), synaptosome (Syn), and PSD fractions of whole brain, cortex, cerebellum, or hippocampus (equal protein loading) show that Myo6 is enriched in the PSD fraction throughout the brain. Controls for both preparation purity and gel loading included postsynaptically enriched NMDA-R1 and PSD-95, as well as presynaptically enriched synaptophysin (Synphys). Lanes on the same blot are shown separated for easier comparison. (C) Isolated PSD and TX-permeabilized synaptosome (Syn) fractions were incubated in the presence or absence of ATP, and the pellet (P) and supernatant (S) fractions were equal volume loaded. The majority of Myo6 in the PSD fraction, but not the synaptosome fraction, was pelleted despite ATP treatment.

fraction, suggesting that most synaptic Myo6 associates with F-actin alone (Fig. 2 C).

Sv/sv hippocampus exhibits synaptic abnormalities

To determine whether disruption of Myo6 results in any synaptic deficits in vivo, we performed EM analyses on *sv/sv* brain. Specifically, we examined hippocampal area CA1, as it is rich in spiny pyramidal cell dendrites and very well characterized with respect to dendritic ultrastructure (Harris and Landis, 1986; Hering and Sheng, 2001). The inner ear hair cell deficits in *sv/sv* mice lead to a degeneration of the neurosensory epithelium, resulting in deafness and severe vestibular dysfunction (Avraham et al., 1995). Thus, to control for secondary effects in *sv/sv* brain, we included myosin VIIa (Myo7a) mutant (*Shaker-1*; *sh1/sh1*) mice in our analyses. These mice, which express normal levels of Myo6, are also deaf and exhibit identical spinning behavior, but are unlikely to have significant central nervous system defects because there is a negligible amount of Myo7a expressed in brain (Hasson et al., 1995). We find that

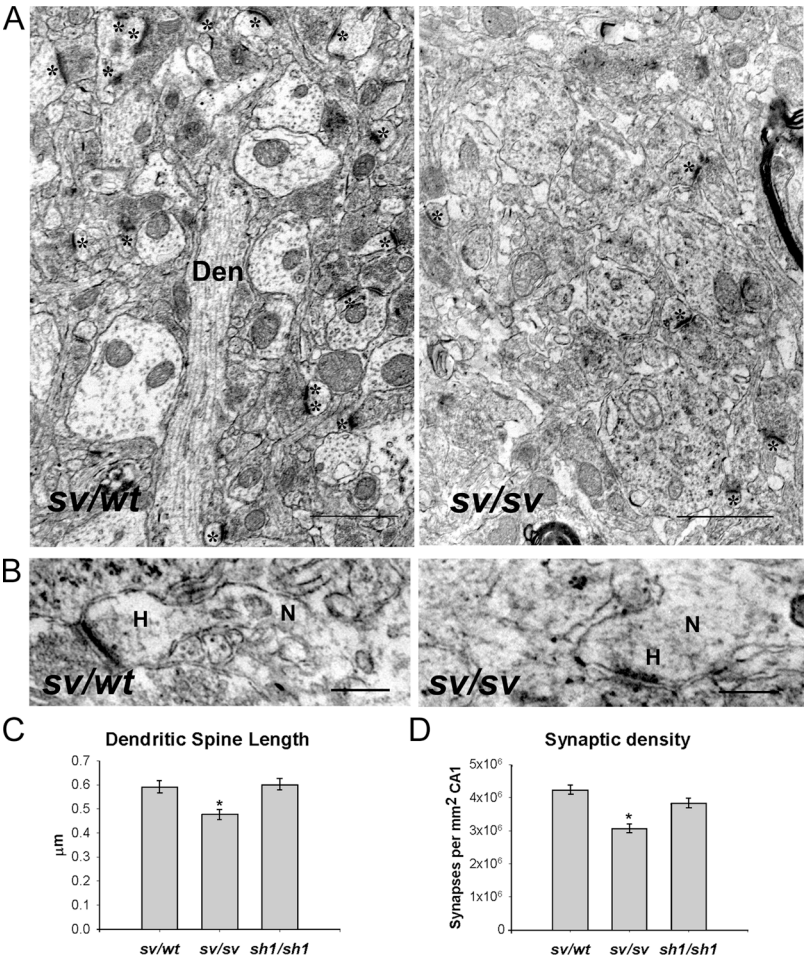

Figure 3. ***Sv/sv* mice have fewer synapses and shorter dendritic spines in CA1.** (A) Representative images show that *sv/sv* CA1 displays abnormal morphology, including fewer synapses per square millimeter, than *sv/wt* CA1. Dendrites (Den) and synapses (*) are labeled. Bars, 1 μm. (B) Dendritic spines in *sv/sv* CA1 are shorter than those in *sv/wt* CA1. Dendritic spine heads (H) and necks (N) are labeled. Bars, 0.25 μm. Minimal contrast/brightness adjustment was performed. (D) Quantification of random images reveals that *sv/sv* CA1 has 27% fewer synapses per square millimeter as compared with *sh1/sh1* or *sv/wt* CA1 (*, $P < 0.001$; $n_{sv/sv} = 87$, $n_{sv/wt} = 57$, and $n_{sh1/sh1} = 77$). (C) Length measurements of multiple dendritic spines from *sv/wt*, *sv/sv*, and *sh1/sh1* CA1 show that *sv/sv* CA1 dendritic spines are an average of 19% shorter than *sh1/sh1* and *sv/wt* spines (*, $P < 0.001$; $n_{sv/sv} = 94$, $n_{sv/wt} = 103$, and $n_{sh1/sh1} = 98$). Error bars indicate SEM.

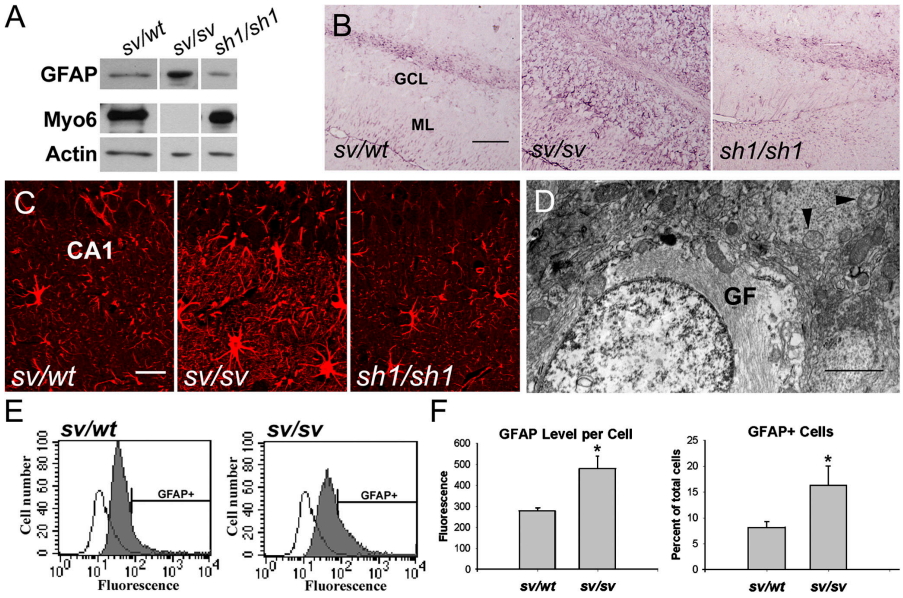

Figure 4. ***Sv/sv* mice display astrogliosis throughout the brain.** (A) Western blots of *sv/wt*, *sv/sv*, and *sh1/sh1* brain homogenates, equal protein loaded, reveal that GFAP is increased fourfold in *sv/sv* versus *sv/wt* brain. Densitometric analysis compared the ratios of GFAP to actin between samples. Lanes between those shown were omitted. (B and C) *Sv/sv*, *sv/wt*, and *sh1/sh1* brain sections were incubated with anti-GFAP, and either peroxidase- (B) or fluorescence (C)-conjugated secondary antibody. Representative images of cerebellum (B) and hippocampus (C) depict the greater GFAP immunoreactivity seen in *sv/sv* versus *sv/wt* and *sh1/sh1* brains. Granule cell (B, GCL) and molecular layers (B, ML) of the cerebellum and area CA1 of the hippocampus (C) are labeled. Bars: (B) 0.25 mm; (C) 20 μm. Minimal contrast/brightness adjustment was performed. (D) Activated astrocyte exhibiting prominent gliofilaments (GF) characteristic of *sv/sv* neuropil. Swollen mitochondria (arrowheads) are seen in surrounding cells. Bar, 1 μm. (E) Cells isolated from *sv/wt* or *sv/sv* brains were analyzed by flow cytometry. Unstained cells (open peaks) were compared with labeled cells (shaded peaks) and used to determine background fluorescence (not within the GFAP+ region). (F) The proportion of cells within the GFAP+ range and the mean label intensity within this range were compared, and reveal that *sv/sv* mice have a 2.1-fold increase in GFAP+ astrocytes (*, $P < 0.05$, $n = 4$ each) per 100,000 cells and a 1.7-fold increase in GFAP per cell (*, $P < 0.02$, $n = 4$ each). Error bars indicate SEM.

the ultrastructure of *sv/sv* CA1 is markedly different from those of Myo6 heterozygous (*sv/wt*) and *sh1/sh1* controls. A noticeable decrease in synapses is observed, and quantification reveals that *sv/sv* mice have 27% fewer synapses per square millimeter of CA1 than *sv/wt* and *sh1/sh1* mice (Fig. 3 D; $P < 0.001$). In addition to synapse number, we examined the morphological features of *sv/sv* dendritic spines. Specifically, we measured dendritic spine lengths, head widths, neck widths, PSD lengths, and two-dimensional surface areas in multiple images of CA1. Of these parameters, dendritic spine length was the only measure that was significantly different, with *sv/sv* CA1 dendritic spines 19% shorter than those of *sv/wt* and *sh1/sh1* controls (Fig. 3 C; $P < 0.001$).

Sv/sv brain displays widespread astrogliosis

Ultrastructural studies reveal that in addition to exhibiting synaptic deficits, *sv/sv* neuropil is highly disordered compared with control neuropil (Fig. 3 A). Further investigation revealed that this is likely caused by an increased number of astrocytes in *sv/sv* brain. Astrocytes can be distinguished from most other cells by the expression of the filament protein glial fibrillary acidic protein (GFAP). Immunoblotting of *sv/sv* brain shows a fourfold increase in GFAP, as compared with *sv/wt* brain, though no increase was seen in *sh1/sh1* brain (Fig. 4 A). Increased GFAP can also be detected by immunostaining of *sv/sv* brain (Fig. 4, B and C), and the abundance of GFAP-labeled processes seen throughout *sv/sv* CA1 (Fig. 4 C) may account for its disordered appearance by EM (Fig. 3). Indeed, further EM analyses revealed the presence of many gliofilament-containing astrocytes within *sv/sv* CA1 (Fig. 4 D).

Astrocytes up-regulate GFAP and proliferate in response to central nervous system injuries such as stroke, epilepsy, or neurodegenerative disease, a process termed astrogliosis (Little and O'Callagha, 2001). To verify that the increased GFAP observed in *sv/sv* brain was caused by an increase in GFAP per astrocyte, and not solely by an increase in astrocyte number, we performed flow cytometry on cells isolated from *sv/sv* brain. Flow cytometry has been reliably used to assess the proportions of different cell types in both whole brain and culture (Tomomura et al., 2001; Sergent-Tanguy et al., 2003). Because the level of GFAP in *sh1/sh1* brain does not differ from that in *sv/wt* brain (Fig. 4, A–C), we excluded this group from our flow cytometric analyses. After isolation and staining, the proportion and mean fluorescence intensity of GFAP-positive (GFAP+) cells in each brain were determined by cell sorting (Fig. 4 E). Analyses revealed that *sv/sv* brain exhibits a 2.1-fold increase in the proportion of GFAP+ cells ($P < 0.05$) and a 1.7-fold increase in GFAP per cell ($P < 0.02$), compared with *sv/wt* littermates (Fig. 4 F). These results indicate that both the astrocytic up-regulation of GFAP and the number of astrocytes are increased in *sv/sv* brain.

Disruption of Myo6 in hippocampal neurons results in decreased synaptic density

To determine whether the synaptic deficits seen in *sv/sv* brain are caused solely by astrogliosis, we examined *sv/sv* hippocampal neurons isolated in cell culture. These neurons exhibit no obvious morphological changes, and mature to an age at which synaptic structure can be observed. However, analyses of synaptic density revealed that *sv/sv* neurons express 21% fewer PSD-95–labeled synapses than *sv/wt* neurons (Fig. 5, A–C; $P < 0.001$). In addition, analyses of spinophilin staining revealed that *sv/sv* neurons express 22% fewer spinophilin-labeled dendritic spines than *sv/wt* neurons (Fig. 5, D–F; $P < 0.001$). It is unlikely that this deficit is caused by altered regulation of spinophilin, as Myo6 does not interact with spinophilin in rat brain and levels of spinophilin are not altered in *sv/sv* brain (unpublished data). To determine whether synapse loss could be induced with acute disruption of Myo6, we examined cultured

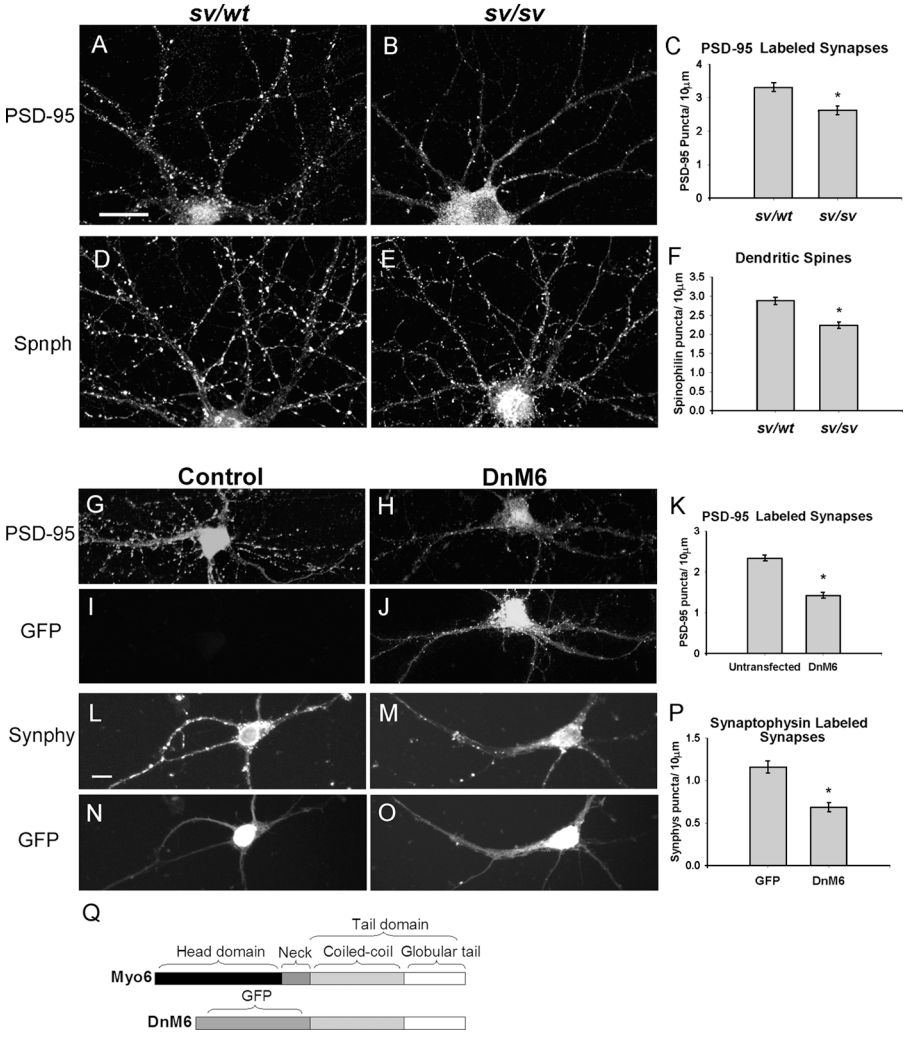

Figure 5. **Myo6-deficient neurons have fewer synapses and dendritic spines.** (A–F) Hippocampal neurons (at 14–21 d) from *sv/sv* and *sv/wt* embryos were stained for PSD-95 or spinophilin (Spnph). Quantification reveals that *sv/sv* neurons have 21% fewer PSD-95–labeled synapses (*, $P < 0.001$; $n_{sv/sv}$ = 147 and $n_{sv/wt}$ = 160) and 22% fewer dendritic spines (*, $P < 0.001$; $n_{sv/sv}$ = 165 and $n_{sv/wt}$ = 126) than *sv/wt* neurons. (G–P) Rat hippocampal neurons (at 14 d) were transfected with dnM6 or EGFP. DnM6 expression is concentrated at the cell body and in bright clusters throughout the dendrite. Cultures were stained for PSD-95 (G–J) or synaptophysin (Synphy; L–O). Minimal contrast/brightness adjustment was performed. Quantification revealed the following: neurons expressing dnM6 have (K) 39% fewer PSD-95–labeled synapses than untransfected neurons in the same dish (*, $P < 0.001$; n_{dn} = 146 and n_{un} = 148) and (P) 41% fewer synaptophysin-labeled synapses than neurons expressing EGFP (*, $P < 0.001$; n_{dn} = 126 and n_{GFP} = 93). (Q) Schematic of Myo6 domain structure. DnM6 contains an EGFP tag NH_2-terminal to the tail of Myo6. Bars, 10 μm. Error bars indicate SEM.

hippocampal neurons expressing an EGFP-tagged dnM6 (Fig. 5 Q). This dnM6 has been shown to specifically disrupt native Myo6 function in nonneuronal cells (Aschenbrenner et al., 2003). In hippocampal neurons, dnM6 localizes to discrete clusters throughout the dendrites and cell bodies (Fig. 5 J), which is consistent with endogenous Myo6 staining (Fig. 2 A). We find that neurons expressing dnM6 have 39% fewer PSD-95–labeled synapses, as compared with untransfected neurons in the same dish (Fig. 5, G–K; $P < 0.001$). Consistent with this, dnM6-expressing neurons display a 41% decrease in synaptophysin-labeled synapses, as compared with neurons expressing EGFP alone (Fig. 5, L–P; $P < 0.001$). The greater synapse loss seen in dnM6-expressing, versus *sv/sv*, neurons may reflect the difference between an acute versus chronic loss of Myo6 function. Indeed, mature neurons transfected with dnM6 are not likely to develop the compensatory mechanisms that are developed by *sv/sv* neurons. These results suggest that Myo6 function is important for mature hippocampal synapses.

Myo6 interacts with the AMPAR, AP-2, and SAP97 in rat brain

The abnormalities seen in *sv/sv* neurons prompted us to investigate possible roles for Myo6 at the PSD. At stimulated synapses, AMPARs undergo regulated, clathrin- and AP-2–mediated endocytosis (Carroll et al., 1999; Luscher et al., 1999). Given its proposed function in nonneuronal cells and its association with SAP97 (Wu et al., 2002), we questioned whether Myo6 functions in AMPAR endocytosis. To explore this, we performed immunoprecipitation (IP) experiments from a deoxycholate (DOC)-extracted, dendrite-rich fraction of rat brain. The use of DOC was necessary, given the insolubility of PSD proteins; however, DOC may interfere with some protein–protein interactions (Naisbitt et al., 2000). Despite these conditions, Myo6 coimmunoprecipitates with both the GluR1 and GluR2 subunits of the AMPAR in this extract (Fig. 6 A). This complex also contains SAP97 and AP-2. Interestingly, this interaction is specific, as Myo6 does not coimmunoprecipitate with the NR2B and NR1 subunits of the NMDAR, despite the presence of SAP97 (Fig. 6 A). Supporting these data, IP of SAP97 brings down Myo6, AP-2, and the AMPAR (Fig. 6 B). These results indicate that Myo6 specifically interacts with endocytic AMPARs, and that this interaction can withstand the presence of an ionic detergent.

Sv/sv neurons display defective AMPAR internalization

To directly assess whether Myo6 plays a role in AMPAR endocytosis, we used a well-characterized assay system designed to measure stimulus-induced AMPAR internalization in mature

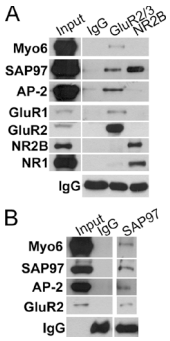

Figure 6. **Myo6 exists in a complex with the AMPAR, AP-2, and SAP97 in rat brain.** (A) IP of the AMPAR from DOC-extracted rat brain brings down Myo6, SAP97, and AP-2. Both GluR2 and GluR1 subunits are present in this complex. Myo6 does not coimmunoprecipitate with the NR2B and NR1 subunits of the NMDAR, despite the presence of SAP97 in this complex. (B) SAP97 immunoprecipitates a complex containing Myo6, AP-2, and the AMPAR. IPs done with equal amounts of nonimmune IgG are devoid of Myo6. Input lanes are 0.1 vol relative to IP lanes.

hippocampal neurons (Carroll et al., 1999; Snyder et al., 2001). *Sv/sv* and *sv/wt* hippocampal neurons were incubated with antibody specific for the extracellular domain of the GluR1 subunit of the AMPAR and stimulated with 100 μM AMPA for 15 min. After stimulation, surface-bound antibody was removed with a strip buffer, and the neurons were fixed, permeabilized, and incubated with a fluorescent secondary antibody. This protocol results in visualization of only the antibody-bound receptors internalized during AMPA treatment (Carroll et al., 1999; Snyder et al., 2001). Consistent with previous reports (Carroll et al., 1999; Lin et al., 2000), our control group (*sv/wt* neurons) displays an 83% increase in AMPAR internalization after AMPA treatment (Fig. 7, G, H, and K; $P < 0.001$). However, in *sv/sv* neurons, no AMPAR internalization was observed after AMPA stimulation (Fig. 7, I–K). To further explore the deficit seen in *sv/sv* neurons, we repeated our experiments using insulin, which has also been shown to induce AMPAR endocytosis

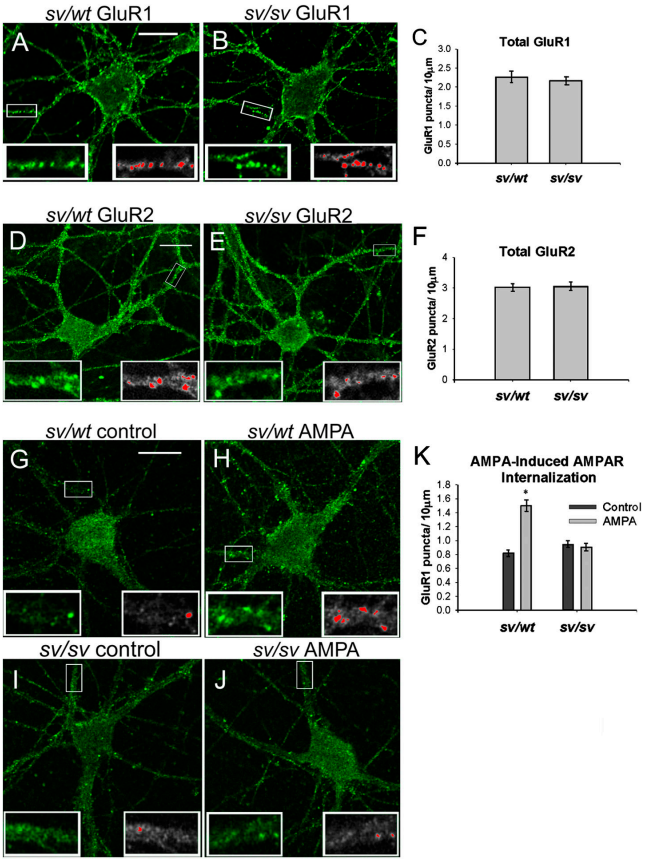

Figure 7. ***Sv/sv* hippocampal neurons display dysfunctional AMPA-induced AMPAR internalization.** (A–F) Total GluR1 ($n_{sv/wt}$ = 183 and $n_{sv/sv}$ = 173) or GluR2 ($n_{sv/sv}$ = 114 and $n_{sv/wt}$ = 115) was measured in unstimulated neurons by permeabilization and incubation with secondary antibody, and both were found to be the same in *sv/wt* and *sv/sv* neurons. (G–J) GluR1 antibody was applied for 10 min, followed by 1 μM TTX ± 100 μM AMPA for 15 min. Internalized AMPARs were assessed after incubation with acetic acid followed by permeabilization and secondary incubation. (K) AMPA treatment induces an 83% increase in internalized AMPARs in *sv/wt* neurons (*, $P < 0.001$; n_{con} = 171 and n_{AMPA} = 156), but no increase in *sv/sv* neurons (n_{con} = 148 and n_{AMPA} = 125). Bars, 10 μm. Error bars indicate SEM. Insets show (left) enlarged areas of dendrite and (right) puncta counted (red) based on thresholding of images. Minimal contrast/brightness adjustment was performed.

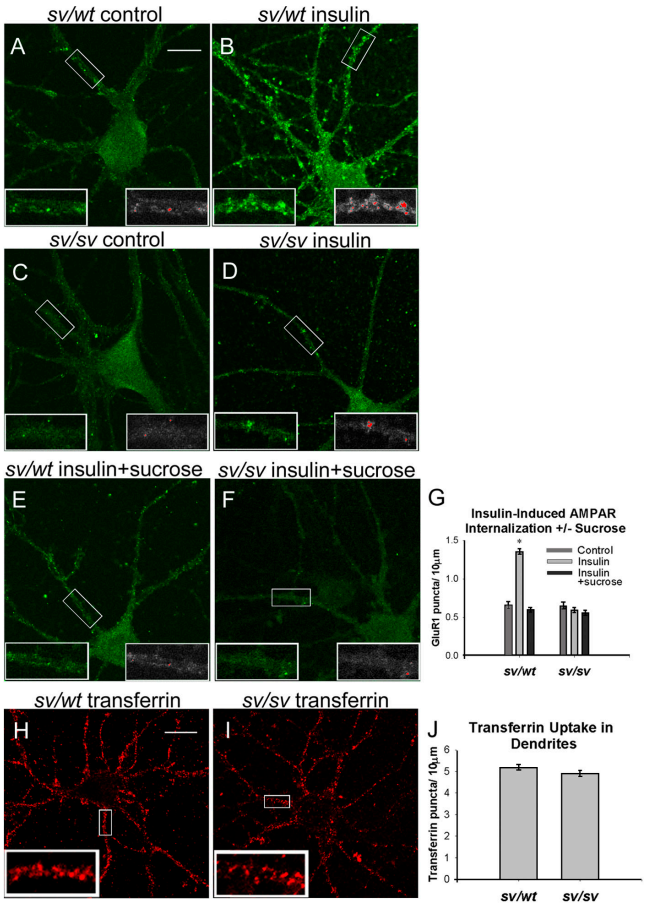

Figure 8. ***Sv/sv* hippocampal neurons display dysfunctional insulin-induced AMPAR internalization identical to the disruption of clathrin-mediated endocytosis.** (A–F) Anti-GluR1 was applied for 10 min, followed by 1 μM TTX ± 10 μM insulin for 15 min. Clathrin-mediated endocytosis was disrupted with a 10-min incubation in 0.45 M sucrose before stimulation. Internalized AMPARs were assessed after incubation with acetic acid followed by permeabilization and secondary incubation. Minimal contrast/brightness was performed. Insets show puncta counted (red) based on thresholding of images. (G) Insulin treatment induces a 106% increase in internalized AMPARs in *sv/wt* neurons (*, $P < 0.001$; n_{con} = 139 and n_{ins} = 170), but no change in *sv/sv* neurons (n_{con} = 161 and n_{ins} = 110). (E and F) Inhibition of clathrin-mediated endocytosis diminishes AMPAR internalization to control levels in insulin-stimulated *sv/wt* neurons ($n_{ins + suc}$ = 188), but does not affect insulin-stimulated *sv/sv* neurons ($n_{ins + suc}$ = 159). Insets show (left) enlarged areas of dendrite and (right) puncta counted based on thresholding of images. Minimal contrast/brightness was performed. (H–J) Dendritic uptake of Alexa 568–labeled Tf is similar in *sv/wt* and *sv/sv* neurons ($n_{sv/sv}$ = 273 and $n_{sv/wt}$ = 215). Insets show (left) enlarged areas of dendrite and (right) puncta counted (red) based on thresholding of images. Minimal contrast/brightness was performed. Bars, 10 μm. Error bars indicate SEM.

in a clathrin-dependent manner (Lin et al., 2000; Man et al., 2000). A 15-min stimulation with 10 μM insulin resulted in a 106% increase in AMPAR internalization in *sv/wt* neurons (Fig. 8, A, B, and G; $P < 0.001$). AMPAR internalization in insulin-treated *sv/sv* neurons, however, was no different from that in unstimulated neurons (Fig. 8, C, D, and G).

To determine whether this deficit in AMPAR internalization is caused by a decreased steady-state expression of GluR1, we examined total GluR1 levels in *sv/sv* and *sv/wt* neurons. Analyses revealed no difference in total GluR1 levels between *sv/sv* and *sv/wt* neurons (Fig. 7, A–C). In addition, we measured the levels of surface-expressed GluR1 in *sv/sv* neurons at steady state, and found that they do not differ from levels in *sv/wt* neurons (unpublished data). The internalization of GluR1 is likely mediated by its association with the GluR2 subunit of the AMPAR (Man et al., 2000). Therefore, we examined the steady-state level of GluR2 in *sv/sv* hippocampal neurons. Similar to those of GluR1, total GluR2 levels are not different between *sv/sv* and *sv/wt* neurons (Fig. 7, D–F).

It is reasonable to hypothesize that disruption of Myo6 trafficking of clathrin-coated vesicles is responsible for the dysfunctional AMPAR internalization seen in *sv/sv* neurons. To verify that our assay specifically measured clathrin-mediated endocytosis, we pretreated neurons with 0.45 M hypertonic sucrose, and stimulated them again with insulin. This treatment has been shown to disrupt clathrin-mediated endocytosis and abolish AMPAR internalization in hippocampal neurons (Hansen et al., 1993; Man et al., 2000). Consistent with previous findings, sucrose preincubation reduced the AMPAR internalization in insulin-treated *sv/wt* neurons to background levels (Fig. 8, E and G). In addition, sucrose preincubation had no further effect on *sv/sv* neurons (Fig. 8, F and G).

This result confirms that our assay system is specifically measuring clathrin-mediated endocytosis, and suggests that the deficit seen in *sv/sv* neurons is caused by a deficit in clathrin-mediated endocytosis. However, if Myo6 were essential for all clathrin-mediated endocytosis at synapses, greater deficits would be expected. To explore whether Myo6 disruption results in a general deficit in clathrin-mediated endocytosis, we examined Alexa 568–labeled Tf uptake in *sv/sv* dendrites. Interestingly, dendritic uptake of Alexa 568–labeled Tf is the same in *sv/sv* and *sv/wt* neurons (Fig. 8, H–J), which suggests that the involvement of Myo6 in clathrin-mediated endocytosis is specific for certain targets, such as the AMPAR.

Discussion

Myosin transport of proteins and organelles along F-actin underlies the most basic of cellular processes. At the actin-rich dendritic spine, this transport is especially important for the spatial and temporal coordination of glutamate receptors and signaling molecules that participate in excitatory synaptic transmission. The localization of Myo6 at the PSD, with its unique properties, has significant implications for synaptic function. Our results show that a loss of Myo6 leads to a decrease in synaptic density and dendritic spine abnormalities in whole brain and isolated hippocampal neurons. Similarly, hippocampal neurons expressing dnM6 exhibit a decrease in synapse number, which suggests that acute Myo6 disruption at mature synapses results in their elimination. In addition, *sv/sv* brain exhibits widespread astrogliosis. Finally, we find that *sv/sv* neurons display a specific deficit in the stimulation-induced internalization of AMPARs, which is mimicked by the disruption of clathrin-mediated endocytosis in *sv/wt* neurons. Supporting this, Myo6 exists in a complex with the AMPAR, SAP97, and AP-2 in rat brain.

Myo6 and AMPAR internalization

The results reported here indicate that Myo6 links AMPAR internalization to the postsynaptic cytoskeleton. Consistent with this, EM imaging of myosin-decorated F-actin in dendritic spines suggests that it is polarized, with plus ends pointed toward the plasma membrane (Fifkova and Delay, 1982). This arrangement would allow minus end–directed Myo6 to pull endocytic AMPARs down from the dendritic spine surface. Supporting this, our results demonstrate that Myo6 exists in a complex with AP-2, which has previously been shown to play a role in AMPAR internalization (Carroll et al., 1999). Furthermore, our results suggest that Myo6 interacts specifically with endocytic AMPARs, as it does not coimmunoprecipitate with the NMDAR in rat brain. Consistent with this, constitutive Tf uptake is not disrupted in *sv/sv* neurons, which suggests that Myo6 does not function in all clathrin-mediated endocytosis events at the PSD. Instead, Myo6 may selectively target clathrin pits containing AMPARs. Such specificity could be mediated by specialized adaptor proteins such as SAP97 and AP-2.

The regulation of AMPAR expression at the PSD is thought to be an important component of synaptic plasticity, or the long-term modification of synaptic strength, which has been linked to learning and memory (Malinow and Malenka, 2002). Recent evidence suggests that the coordinated endocytosis of AMPARs directly mediates long-term depression (LTD), a form of synaptic plasticity. Induction of LTD in hippocampal neurons in vitro and in vivo results in decreased AMPAR expression at the plasma membrane (Heynen et al., 2000). Furthermore, inhibition of clathrin-mediated endocytosis of AMPARs blocks the induction of LTD in hippocampal neurons (Luscher et al., 1999; Man et al., 2000). Given this, our results suggest that the Myo6-dependent internalization of AMPARs may play an important role in the induction or maintenance of LTD.

The loss of synapses observed in *sv/sv* neurons may appear to be inconsistent with unaltered levels of GluR1 and GluR2 at steady state. However, decreased synapse number in *sv/sv* neurons may result in a redistribution of AMPARs to extrasynaptic sites without affecting total AMPAR number. Indeed, overexpression of PSD-95 causes an increase in synaptic AMPARs without altering the overall expression of AMPARs at the surface, whereas overexpression of the protein stargazin causes an increase in extrasynaptic AMPARs without changing the number of synaptic AMPARs (Schnell et al., 2002). In addition, disruption of F-actin in cultured neurons has been shown to lead to a dramatic decrease in the number of synaptic AMPARs without changing the number of PSD-95 clusters,

suggesting that AMPAR trafficking occurs independent of the synapse (Allison et al., 1998). Thus, the synapse loss observed in *sv/sv* neurons would not necessarily be reflected in an overall decrease in AMPAR number.

Abnormalities in *sv/sv* brain

The synaptic deficits and astrogliosis observed in *sv/sv* brain are intriguing, and how they result from a loss of Myo6 is unclear. There may be interactions of Myo6 with proteins other than the AMPAR at the PSD, and the loss of these might contribute to the deficits observed in *sv/sv* brain. In addition, it is important to note that Myo6 has been localized to axons in developing neurons (Suter et al., 2000), and our results indicate that Myo6 expression is not restricted to the PSD at adult synapses (Fig. 2 C). Thus, it is possible that our results may partially reflect a loss of Myo6 function in the presynaptic terminal.

However, there is much evidence to suggest that dysfunctional glutamate receptor regulation results in abnormalities similar to those seen in *sv/sv* brain. Specifically, inefficient internalization of AMPARs, as is seen in *sv/sv* neurons, has been shown to result in increased excitatory current in hippocampal slices (Luscher et al., 1999). Such excessive activation of glutamate receptors has in turn been shown to lead to dendritic spine loss within 10 min of agonist application, even at sublethal levels (Halpain et al., 1998; Hasbani et al., 2001). Consistent with this, dendritic spine loss and decreased dendritic spine length are seen in cases of epilepsy, which is a disorder characterized by excessive excitatory signaling (Fiala et al., 2002). In addition, specific inhibition of AMPAR signaling has been shown to lead to both loss and shortening of dendritic spines (McKinney et al., 1999). Astrogliosis is also associated with excessive glutamatergic signaling. Injection of NMDA (Burtrum and Silverstein, 1993) or kainic acid (Chen et al., 2002) in rodents results in robust and sustained astrogliosis. Supporting this, astrogliosis is commonly seen in cases of epilepsy (Pitkanen and Sutula, 2002).

Despite an increase in astrocyte number, we do not see an appreciable difference in the size of *sv/sv* brain. This is consistent with studies showing that astrogliosis does not necessarily correlate with an increase in brain volume (Sykova et al., 2002). Instead, astrocytes may occupy space that once contained neurons, which have since degenerated. Indeed, our EM analyses reveal features of cellular degeneration in *sv/sv* neuropil, such as swollen mitochondria (Fig. 4 D). Interestingly, swollen mitochondria often signify dysfunctional calcium regulation, and can be induced in cultured neurons with excessive glutamate application (Isaev et al., 1996). Further investigation of the astrogliosis in *sv/sv* brain is currently underway.

Materials and methods

Antibodies

10 μg/ml anti-Myo6 was raised against Myo6 tail (Hasson and Mooseker, 1994). Antispinophilin (1:1,000) was a gift from P. Allen (Yale University, New Haven, CT). The following commercial antibodies were used: nonimmune IgG (Jackson ImmunoResearch Laboratories); mAbs to synaptophysin (2 μg/ml; CHEMICON International), PSD-95 (2 μg/ml; Upstate Biotechnology), NR1 (BD Biosciences), GluR2 (CHEMICON International), SAP97 (StressGen Biotechnologies), β-adaptin (BD Biosciences), actin (CHEMICON International), and GFAP (1:500; CHEMICON International); polyclonal antibodies to GluR1 (Oncogene Research Products), GluR2/3 (Upstate Biotechnology), NR2B (Upstate Biotechnology), and GFAP (1:1,000; CHEMICON International); and goat anti–mouse Alexa 488, goat anti–rabbit (GaR) Alexa 568, and GaR Alexa 488 (1:500, except for internalization assays; Molecular Probes, Inc.).

Mice

Sv/wt (*Myo6^{sv}/J*) and *sh1/wt* (*Myo7a$^{sh1\text{-}8J}$/J*) mice were purchased from The Jackson Laboratory, and colonies of both were established. Original heterozygous mice were bred to produce homozygous mice. As homozygous mice do not breed, all animals used for experiments were obtained through homozygous/heterozygous breeding pairs. With the exception of those used in hippocampal cultures, all mice used were male, to avoid estrogen-related dendritic spine changes that occur during estrus (Woolley and Schwartzkroin, 1998), and age-matched within each experiment. All experimental protocols have been approved by the Yale Institutional Animal Care and Use Committee.

Immunohistochemistry

1-yr-old C57/B6J mice (The Jackson Laboratory) were perfuse-fixed (at RT; 4% PFA/PBS; Electron Microscopy Sciences). Frozen 10-μm sections were taken with a freezing microtome, and 5-μm paraffin sections were deparaffinized and processed for antigen retrieval as described previously (Shi et al., 1997). Sections were incubated in block buffer (BB; 5% normal goat serum [Sigma-Aldrich], 5% BSA [Sigma-Aldrich], and 10% horse serum [Hyclone] in PBS) with 1% TX for 1 h at 37°C and primary antibody (or nonimmune IgG) in BB/0.1% TX for 1 h at 37°C or overnight at 4°C, and stained with the VECTASTAIN Elite ABC peroxidase system (Vector Laboratories) or GaR Alexa 568 in BB/0.1% TX for 30 min at RT.

PSD and synaptosome preparations

PSD preparations were performed at 4°C as described previously (Dosemeci and Reese, 1993). All solutions contained 1 mM Pefabloc and 1 mM DTT. In brief, C57/B6J mouse brains or Lewis rat brain regions were homogenized in 0.32 M sucrose with a Teflon dounce and cleared at 1,400 *g*, and the supernatant was spun at 13,800 *g* for 10 min. The pellet was resuspended and run over a discontinuous sucrose gradient (1.2 M/1 M/0.85 M) at 82,500 *g* for 2 h, and the 1.2 M/1 M interface (synaptosome fraction) was collected, solubilized in 0.5% TX for 15 min at RT, and spun at 36,000 *g* for 30 min. The pellet was then run over a second gradient (2.1 M/1.5 M/1 M) for 20 min at 200,000 *g*, and the 2.1 M/1.5 M interface was collected, incubated with 75 mM KCl and 0.5% TX, run over a 2.1-M sucrose cushion, washed with 20 mM Hepes, and run over a second cushion.

ATP extractions

Isolated synaptosome and PSD fractions were resuspended in buffer A (1 mM EGTA, 75 mM KCl, 2.5 mM $MgCl_2$, 1 mM DTT, 1 mM Pefabloc, and 20 mM imidazole, pH 7.2) or in 50 mM Mg-ATP (50 mM ATP and 50 mM $MgCl_2$), or dH_2O was added (1:10; for synaptosomes, 0.1% TX was also added), and they were incubated for 30 min at 37°C. Fractions were then spun at 200,000 *g* for 30 min, the supernatants were removed, the pellets were resuspended to their original volumes with buffer A, and both fractions were loaded equal volume. These experiments were repeated three times.

IP

DOC-solubilized extracts were made from adult rat brain, essentially as described previously (Naisbitt et al., 2000). Extracts were precleared with 0.1 vol protein A–Sepharose (Amersham Biosciences) for 1 h at 4°C and incubated with 10 μg/ml of antibodies to GluR2/3, NR2B, or SAP97, or with nonimmune IgG, overnight at 4°C. Protein A–Sepharose was then added (1:10), and the extracts were incubated for 1 h at 4°C. Pellets were washed five times for 1 min with HSIPB (10 μg/ml BSA, 1 mM DTT,1 mM EGTA, 200 mM KCl, 5 mM Mg-ATP, 1 mM Pefabloc, 50 mM Tris, pH 7.4, and 0.1% TX) and processed for SDS-PAGE.

Western blotting

The protein concentration of each sample was determined using a colorimetric assay (BCA; Pierce Chemical Co.) and densitometric analysis of a Coomassie blue–stained gel that was performed using the one-dimensional gel analysis tool in Metamorph 5.0 (Universal Imaging Corp.). Samples were run on 5–20%-gradient SDS-PAGE gels and transferred (at 85 V for 2–4 h at 4°C) to nitrocellulose. Immunoblotting was performed with the appropriate primary antibodies and ECL, according to the kit instructions (Amersham Biosciences). Densitometry was performed on

scanned blot films using the gel analyzer tool in Image J. The density of the GFAP band was expressed as a percent of the actin band in the same lane, and this ratio was compared among *sv/wt*, *sv/sv*, and *sh1/sh1* samples.

Immunocytochemistry

Cultures of rat hippocampal neurons were made as described previously (Goslin and Banker, 1991). In brief, embryonic day 18 rat hippocampus was dissected, incubated in 0.25% trypsin at 37°C, and dissociated by trituration, and 100,000–200,000 cells/ml were plated onto 1 mg/ml poly-L-lysine–coated glass coverslips for 3 h at 37°C. The coverslips were then inverted over a monolayer of glial cells in modified N2 medium and kept in vitro for 14–21 d. For staining, live-cell extraction was performed to enhance staining of nonsoluble elements (i.e., PSD components), as described previously (Suter et al., 2000). In brief, coverslips were incubated in 0.05% saponin in PHEM buffer (60 mM Pipes, 25 mM Hepes, pH 7, 5 mM EGTA, and 3% sucrose) for 30 s at 37°C, 4% PFA/0.1% TX/PHEM for 10 min at 37°C, 4% PFA/PHEM for 30 min at 37°C, BB for 30 min at RT, primary antibody in BB overnight at 4°C, and secondary antibody in BB for 30 min at RT, and were mounted with ProLong antifade (Molecular Probes, Inc.). For synaptophysin staining, cells were fixed in 4% PFA/4% sucrose/PBS for 15 min at 37°C, permeabilized in 0.1% TX/BB for 10 min at RT, and processed for staining as just described.

Internalization assays

Hippocampal neurons from *sv/sv* and *sv/wt* embryos were made as described in the Immunocytochemistry section. All coverslips used were matched for cell density and branching immediately before experimentation. When needed, media were changed to insulin-free or Tf-free modified N2 for at least 8 h. Cells were incubated in 5 μg/ml anti-GluR1 for 10 min at 37°C and stimulated with 100 μM AMPA + 1 μM tetrodotoxin (TTX; Tocris Cookson, Inc.), 10 μM insulin (Sigma-Aldrich) + 1 μM TTX, or N2 + 1 μM TTX, for 15 min at 37°C. Clathrin-mediated endocytosis was disrupted with 0.45 M sucrose for 10 min at 37°C before stimulation. For Tf experiments, coverslips were stimulated with 50 μM Alexa 568 Tf for 10 min at 37°C. Coverslips were then incubated with ice-cold PBS for 1 min (to stop endocytosis) and 0.5 M ice-cold NaCl/0.2 M acetic acid, pH 3.5, for 4 min, washed, fixed, and permeabilized. For AMPA and insulin experiments, coverslips were incubated with GaR Alexa 488 (1:200) in BB for 1 h at RT. To determine total GluR1 and GluR2 levels, unstimulated coverslips were stained in the same way, but without prior exposure to NaCl/acetic acid. Surface GluR1 levels were determined by omitting both the NaCl/acetic acid and permeabilization steps.

Cloning and transfection

The Myo6 tail (starting at the coiled coil; nucleotides 5212–4191; available from GenBank/EMBL/DDBJ under accession no. NM_004999) was obtained by PCR (Herculase; Stratagene) from a cDNA library of human intestinal epithelium. Products were digested with KpnI and BamHI (New England Biolabs, Inc.), cloned into pEGFP-C1 (CLONTECH Laboratories, Inc.), expressed in XL-1 Blue bacteria (Stratagene), and sequenced (Keck Facility, Yale University, New Haven, CT). The resulting construct was transfected into 14-d-old rat hippocampal cultures (Immunocytochemistry section) using lipofectamine 2000 (Invitrogen), and pEGFP-C1 was simultaneously transfected into sister cultures. Cells were returned to glia after 5 h, and left for an additional 19–24 h before staining.

Imaging and data analysis

Sections were imaged with Plan Apo UW 1×/0.04 and Plan Apo 4×/0.2 objectives (Nikon) on an Eclipse microscope (model E800; Nikon) using SPOT imaging equipment and software (SPOT Image Corporation), or with a Plan Apo Chromat 40×/1 objective (Carl Zeiss MicroImaging, Inc.) on a laser scanning confocal microscope (model MRC-1024; Bio-Rad Laboratories), using identical settings for each section in a group. With the exception of those stained for synaptophysin (imaged using a Plan Fluor 20×/0.5 objective [Nikon]), cell staining was imaged with a Plan Apo Chromat 63×/1.4 objective (Carl Zeiss MicroImaging, Inc.) on the aforementioned confocal microscope, using identical settings for each group. Contrast/brightness enhancement and enlargement were done on obtained images only in parallel with control images, using Adobe Photoshop 5.5. In some cases, the background between images was normalized before adjustments were made. For internalization assays, images were taken of 10 randomly selected fields (1–4 cells/field) per coverslip, from three to five independent experiments. Cells from five different transfection experiments were analyzed. Only healthy, process-bearing cells were examined. Using Image J tracing and threshold tools, dendrite length was measured and puncta at least twofold brighter than the background dendrite, with an area of at least five pixels, were counted. These parameters were set based on previous work (Carroll et al., 1999), and we assert, based on careful examination of different parameter definitions, that they accurately reflect the receptor clusters involved in regulated AMPAR endocytosis. In almost all cases, the dendrites measured were primary branches analyzed from the base to the edge of the visual field. In all experiments, *t* tests were performed on normalized data to obtain p-values.

EM

All reagents used were obtained from Electron Microscopy Sciences. Four 1–2-yr-old mice per group were perfuse-fixed as described in the Immunocytochemistry section. CA1 regions (from both hemispheres) were dissected, postfixed in 4% gluteraldehyde/0.1 M sodium phosphate buffer, pH 7.4, overnight at 4°C, washed, immersed in 1% osmium tetraoxide/0.1 M phosphate buffer, pH 6, for 1 h on ice, washed, dehydrated through ethanol, and embedded in Polybed resin. Thin sections were mounted on copper grids, stained, and imaged on an electron microscope (model EM-10; Carl Zeiss MicroImaging, Inc.). Negatives of multiple random 8,000× fields were scanned into Adobe Photoshop 5.5, randomized, and analyzed with Image J. Synapses, identified as dark PSDs opposed to at least three presynaptic vesicles, were counted with the aid of the contrast-adjust and magnification tools in Image J. Images that contained areas devoid of tissue, or that were occluded by contrast or staining artifacts, were discarded. Dendritic spines were identified as dendritic extensions rich in F-actin, devoid of microtubules, and possessing PSDs at their surfaces (Hering and Sheng, 2001). Dendritic spine lengths (from PSD to base), head widths (at widest point), average neck widths, PSD lengths, and surface areas (on a two-dimensional image) were measured using the tracing tools in Image J. Only those spines that were completely longitudinally sectioned, with a clearly visible connection to the dendrite shaft, were measured.

Flow cytometry

Adult (6–10 mo old) *sv/wt* or *sv/sv* brains ($n = 4$ each) were processed for flow cytometry based on previously described protocols (Tomomura et al., 2001; Sergent-Tanguy et al., 2003). In brief, brains were minced with a razor and incubated in 0.25% trypsin in HBSS (GIBCO BRL)/33 mM glucose for 15 min at 37°C, FBS (GIBCO BRL) was added to 10% for 10 min at 37°C, and the mixture was passed through a cell strainer (70-μm pore size; BD Flacon). The flow through was allowed to settle, and the supernatant was decanted. After spinning for 7 min at 200 *g*, cell pellets were resuspended and incubated in 2% PFA, 0.1% TX in BB, BB, anti-GFAP in BB, and goat anti–mouse Alexa 488 (1:200) in BB, and analyzed in 2% FBS/PBS on a FACScalibur, using Cellquest software (Becton Dickinson) as described previously (Sergent-Tanguy et al., 2003). In brief, for each sample, dead cells and debris were gated out based on size and granularity, 100,000 Alexa 488–labeled cells were counted, and histograms of normalized cell number versus fluorescence intensity were created. Positive label was differentiated from background fluorescence based on unstained cells, or cells labeled with nonimmune IgG. Our results were expressed as the proportion of GFAP+ cells in the brain isolate and the average GFAP label intensity per cell.

We thank P. Montero, G. Thomas, and N. Papastathis for maintaining hippocampal cultures, J. Holt for help with FACS, Dr. W. Zhong for use of his imaging equipment, Dr. C. Greer for insightful comments, and all members of the Mooseker lab, especially M. Tyska, V. Mermall, R. Zaarour, and M. Krendel, for helpful discussions.

This work was supported by grants from the National Institute of Diabetes and Digestive and Kidney Diseases (PO1-DK55389 and DK 25387), the National Institute of Mental Health (NS66274-01), the Ellison Medical Foundation (AG-NS-0144-01), and the Patterson Trust.

Submitted: 18 October 2004
Accepted: 22 November 2004

References

Allison, D.W., V.I. Gelfand, I. Spector, and A.M. Craig. 1998. Role of actin in anchoring postsynaptic receptors in cultured hippocampal neurons: differential attachment of NMDA versus AMPA receptors. *J. Neurosci.* 18: 2423–2436.

Aschenbrenner, L., T. Lee, and T. Hasson. 2003. Myo6 facilitates the translocation of endocytic vesicles from cell peripheries. *Mol. Biol. Cell.* 14: 2728–2743.

Avraham, K.B., T. Hasson, K.P. Steel, D.M. Kingsley, L.B. Russell, M.S. Mooseker, N.G. Copeland, and N.A. Jenkins. 1995. The mouse *Snell's waltzer* deafness gene encodes an unconventional myosin required for structural integrity of inner ear hair cells. *Nat. Genet.* 11:369–375.

Berg, J.S., B.C. Powell, and R.E. Cheney. 2001. A millennial myosin census. *Mol. Biol. Cell.* 12:780–794.

Biemesderfer, D., S.A. Mentone, M. Mooseker, and T. Hasson. 2002. Expression of myosin VI within the early endocytic pathway in adult and developing proximal tubules. *Am. J. Physiol. Renal Physiol.* 282:F785–F794.

Bridgman, P.C. 2004. Myosin-dependent transport in neurons. *J. Neurobiol.* 58: 164–174.

Burtrum, D., and F.S. Silverstein. 1993. Excitotoxic injury stimulates glial fibrillary acidic protein mRNA expression in perinatal rat brain. *Exp. Neurol.* 121:127–132.

Buss, F., S.D. Arden, M. Lindsay, J.P. Luzio, and J. Kendrick-Jones. 2001. Myosin VI isoform localized to clathrin-coated vesicles with a role in clathrin-mediated endocytosis. *EMBO J.* 20:3676–3684.

Carroll, R.C., E.C. Beattie, H. Xia, C. Luscher, Y. Altschuler, R.A. Nicoll, R.C. Malenka, and M. von Zastrow. 1999. Dynamin-dependent endocytosis of ionotropic glutamate receptors. *Proc. Natl. Acad. Sci. USA*. 96: 14112–14117.

Chen, Z., H.G. Ljunggren, N. Bogdanovic, I. Nennesmo, B. Winblad, and J. Zhu. 2002. Excitotoxic neurodegeneration induced by intranasal administration of kainic acid in C57BL/6 mice. *Brain Res.* 931:135–145.

Dosemeci, A., and T.S. Reese. 1993. Inhibition of endogenous phosphatase in a postsynaptic density fraction allows extensive phosphorylation of the major postsynaptic density protein. *J. Neurochem.* 61:550–555.

Fiala, J.C., J. Spacek, and K.M. Harris. 2002. Dendritic spine pathology: cause or consequence of neurological disorders? *Brain Res. Brain Res. Rev.* 39: 29–54.

Fifkova, E., and R.J. Delay. 1982. Cytoplasmic actin in neuronal processes as a possible mediator of synaptic plasticity. *J. Cell Biol.* 95:345–350.

Goslin, K., and G. Banker. 1991. Rat hippocampal neurons in low-density culture. *In* Culturing Nerve Cells. G. Banker and K. Goslin, editors. MIT Press, Cambridge. 251–282.

Halpain, S., A. Hipolito, and L. Saffer. 1998. Regulation of F-actin stability in dendritic spines by glutamate receptors and calcineurin. *J. Neurosci.* 18: 9835–9844.

Hansen, S.H., K. Sandvig, and B. van Deurs. 1993. Clathrin and HA2 adaptors: effects of potassium depletion, hypertonic medium, and cytosol acidification. *J. Cell Biol.* 121:61–72.

Harris, K.M., and D.M. Landis. 1986. Membrane structure at synaptic junctions in area CA1 of the rat hippocampus. *Neuroscience.* 19:857–872.

Hasbani, M.J., M.L. Schlief, D.A. Fisher, and M.P. Goldberg. 2001. Dendritic spines lost during glutamate receptor activation reemerge at original sites of synaptic contact. *J. Neurosci.* 21:2393–2403.

Hasson, T. 2003. Myosin VI: two distinct roles in endocytosis. *J. Cell Sci.* 116: 3453–3461.

Hasson, T., and M.S. Mooseker. 1994. Porcine myosin-VI: characterization of a new mammalian unconventional myosin. *J. Cell Biol.* 127:425–440.

Hasson, T., M.B. Heintzelman, J. Santos-Sacchi, D.P. Corey, and M.S. Mooseker. 1995. Expression in cochlea and retina of myosin VIIa, the gene product defective in Usher syndrome type 1B. *Proc. Natl. Acad. Sci. USA*. 92:9815–9819.

Hasson, T., P.G. Gillespie, J.A. Garcia, R.B. MacDonald, Y. Zhao, A.G. Yee, M.S. Mooseker, and D.P. Corey. 1997. Unconventional myosins in inner-ear sensory epithelia. *J. Cell Biol.* 137:1287–1307.

Heintzelman, M.B., T. Hasson, and M.S. Mooseker. 1994. Multiple unconventional myosin domains of the intestinal brush border cytoskeleton. *J. Cell Sci.* 107:3535–3543.

Hering, H., and M. Sheng. 2001. Dendritic spines: structure, dynamics and regulation. *Nat. Rev. Neurosci.* 2:880–888.

Heynen, A.J., E.M. Quinlan, D.C. Bae, and M.F. Bear. 2000. Bidirectional, activity-dependent regulation of glutamate receptors in the adult hippocampus in vivo. *Neuron.* 28:527–536.

Isaev, N.K., D.B. Zorov, E.V. Stelmashook, R.E. Uzbekov, M.B. Kozhemyakin, and I.V. Victorov. 1996. Neurotoxic glutamate treatment of cultured cerebellar granule cells induces Ca^{2+}-dependent collapse of mitochondrial membrane potential and ultrastructural alterations of mitochondria. *FEBS Lett.* 392:143–147.

Kim, C.H., and J.E. Lisman. 1999. A role of actin filament in synaptic transmission and long-term potentiation. *J. Neurosci.* 19:4314–4324.

Lin, J.W., W. Ju, K. Foster, S.H. Lee, G. Ahmadian, M. Wyszynski, Y.T. Wang, and M. Sheng. 2000. Distinct molecular mechanisms and divergent endocytotic pathways of AMPA receptor internalization. *Nat. Neurosci.* 3:1282–1290.

Little, A.R., and J.P. O'Callagha. 2001. Astrogliosis in the adult and developing CNS: is there a role for proinflammatory cytokines? *Neurotoxicology.* 22:607–618.

Luscher, C., H. Xia, E.C. Beattie, R.C. Carroll, M. von Zastrow, R.C. Malenka, and R.A. Nicoll. 1999. Role of AMPA receptor cycling in synaptic transmission and plasticity. *Neuron.* 24:649–658.

Malinow, R., and R.C. Malenka. 2002. AMPA receptor trafficking and synaptic plasticity. *Annu. Rev. Neurosci.* 25:103–126.

Man, H.Y., J.W. Lin, W.H. Ju, G. Ahmadian, L. Liu, L.E. Becker, M. Sheng, and Y.T. Wang. 2000. Regulation of AMPA receptor-mediated synaptic transmission by clathrin-dependent receptor internalization. *Neuron.* 25: 649–662.

McKinney, R.A., M. Capogna, R. Durr, B.H. Gahwiler, and S.M. Thompson. 1999. Miniature synaptic events maintain dendritic spines via AMPA receptor activation. *Nat. Neurosci.* 2:44–49.

Mermall, V., P.L. Post, and M.S. Mooseker. 1998. Unconventional myosins in cell movement, membrane traffic, and signal transduction. *Science.* 279: 527–533.

Mohiddin, S.A., Z.M. Ahmed, A.J. Griffith, D. Tripodi, T.B. Friedman, L. Fananapazir, and R.J. Morell. 2004. Novel association of hypertrophic cardiomyopathy, sensorineural deafness, and a mutation in unconventional myosin VI (MYO6). *J. Med. Genet.* 41:309–314.

Morris, S.M., S.D. Arden, R.C. Roberts, J. Kendrick-Jones, J.A. Cooper, J.P. Luzio, and F. Buss. 2002. Myosin VI binds to and localises with Dab2, potentially linking receptor-mediated endocytosis and the actin cytoskeleton. *Traffic.* 3:331–341.

Naisbitt, S., J. Valtschanoff, D.W. Allison, C. Sala, E. Kim, A.M. Craig, R.J. Weinberg, and M. Sheng. 2000. Interaction of the postsynaptic density-95/guanylate kinase domain-associated protein complex with a light chain of myosin-V and dynein. *J. Neurosci.* 20:4524–4534.

Pitkanen, A., and T.P. Sutula. 2002. Is epilepsy a progressive disorder? Prospects for new therapeutic approaches in temporal-lobe epilepsy. *Lancet Neurol.* 1:173–181.

Redowicz, M.J. 2002. Myosins and pathology: genetics and biology. *Acta Biochim. Pol.* 49:789–804.

Rosenmund, C., and G.L. Westbrook. 1993. Calcium-induced actin depolymerization reduces NMDA channel activity. *Neuron.* 10:805–814.

Schnell, E., M. Sizemore, S. Karimzadegan, L. Chen, D.S. Bredt, and R.A. Nicoll. 2002. Direct interactions between PSD-95 and stargazin control synaptic AMPA receptor number. *Proc. Natl. Acad. Sci. USA*. 99: 13902–13907.

Self, T., T. Sobe, N.G. Copeland, N.A. Jenkins, K.B. Avraham, and K.P. Steel. 1999. Role of myosin VI in the differentiation of cochlear hair cells. *Dev. Biol.* 214:331–341.

Sergent-Tanguy, S., C. Chagneau, I. Neveu, and P. Naveilhan. 2003. Fluorescent activated cell sorting (FACS): a rapid and reliable method to estimate the number of neurons in a mixed population. *J. Neurosci. Methods.* 129:73–79.

Shi, S.R., R.J. Cote, and C.R. Taylor. 1997. Antigen retrieval immunohistochemistry: past, present, and future. *J. Histochem. Cytochem.* 45:327–343.

Snyder, E.M., B.D. Philpot, K.M. Huber, X. Dong, J.R. Fallon, and M.F. Bear. 2001. Internalization of ionotropic glutamate receptors in response to mGluR activation. *Nat. Neurosci.* 4:1079–1085.

Suter, D.M., F.S. Espindola, C.H. Lin, P. Forscher, and M.S. Mooseker. 2000. Localization of unconventional myosins V and VI in neuronal growth cones. *J. Neurobiol.* 42:370–382.

Sykova, E., T. Mazel, R.U. Hasenohrl, A.R. Harvey, Z. Simonova, W.H. Mulders, and J.P. Huston. 2002. Learning deficits in aged rats related to decrease in extracellular volume and loss of diffusion anisotropy in hippocampus. *Hippocampus.* 12:269–279.

Tomomura, M., D.S. Rice, J.I. Morgan, and M. Yuzaki. 2001. Purification of Purkinje cells by fluorescence-activated cell sorting from transgenic mice that express green fluorescent protein. *Eur. J. Neurosci.* 14:57–63.

Warner, C.L., A. Stewart, J.P. Luzio, K.P. Steel, R.T. Libby, J. Kendrick-Jones, and F. Buss. 2003. Loss of myosin VI reduces secretion and the size of the Golgi in fibroblasts from Snell's waltzer mice. *EMBO J.* 22:569–579.

Wells, A.L., A.W. Lin, L.Q. Chen, D. Safer, S.M. Cain, T. Hasson, B.O. Carragher, R.A. Milligan, and H.L. Sweeney. 1999. Myosin VI is an actin-based motor that moves backwards. *Nature.* 401:505–508.

Woolley, C.S., and P.A. Schwartzkroin. 1998. Hormonal effects on the brain. *Epilepsia.* 39:S2–S8.

Wu, H., J.E. Nash, P. Zamorano, and C.C. Garner. 2002. Interaction of SAP97 with minus-end-directed actin motor myosin VI. Implications for AMPA receptor trafficking. *J. Biol. Chem.* 277:30928–30934.

Yamada, K., M. Fukaya, H. Shimizu, K. Sakimura, and M. Watanabe. 2001. NMDA receptor subunits GluRε1, GluRε3 and GluRζ1 are enriched at the mossy fibre–granule cell synapse in the adult mouse cerebellum. *Eur. J. Neurosci.* 13:2025–2036.